Environmental Health Engineering and Management Journal 2016, 3(4), 183–189
http://ehemj.com
doi 10.15171/EHEM.2016.18

Environmental Health Engineering and Management Journal

Original Article

Environmental Health Engineering and Management

Open Access Publish Free

Synthesis of 2,4-dinitrophenylhydrazine loaded sodium dodecyl sulfate-coated magnetite nanoparticles for adsorption of Hg(II) ions from an aqueous solution

Soheil Sobhanardakani[1*], Raziyeh Zandipak[2], Lobat Taghavi[3]

[1]Associate Professor, Department of the Environment, College of Basic Sciences, Hamedan Branch, Islamic Azad University, Hamedan, Iran
[2]Msc, Young Researchers & Elite Club, Hamedan Branch, Islamic Azad University, Hamedan, Iran
[3]Assistant Professor, Department of the Environmental Pollution, College of Environment and Energy, Science and Research Branch, Islamic Azad University, Tehran, Iran

Abstract

Background: The rapid increase in agricultural and industrial development has made heavy metal pollution a serious environmental problem and public health threat; therefore, removal of heavy metals from water is important. The current study prepared DNPH@SDS@Fe_3O_4 nanoparticles as a novel and effective adsorbent for removal of Hg(II) ions from an aqueous solution.

Methods: A selective adsorbent for Hg(II) was synthesized by coating Fe_3O_4 nanoparticles with sodium dodecyl sulfate which was further functionalized with 2,4-dinitrophenylhydrazine (2,4-DNPH). The synthesized nanoparticles were characterized by Fourier transform infrared spectroscopy (FTIR), x-ray diffraction (XRD), scanning electron microscopy (SEM) and SEM–EDXSt. The effects of pH, dose of adsorbent and shaking time on adsorption capacity were investigated. The kinetics and equilibrium of adsorption of the metal ions were thoroughly studied.

Results: SEM showed that the size of the nanoparticles was 20 to 35 nm. The maximum adsorption capacity for Hg(II) was 164.0 mg g^{-1} for an adsorbent dose of 0.04 g at pH 7.0, 25°C and the initial metal concentration was 25 mg L^{-1},which was greater than for most adsorbents previously examined for Hg(II) adsorption. Adsorption experimental data showed good correlation with the pseudo-second-order model and Langmuir isotherm model.

Conclusion: The results indicated that the DNPH@SDS@Fe_3O_4 nanoparticles are an efficient adsorbent for removal of heavy metal from wastewater.

Keywords: Adsorption, Mercury, Magnetite nanoparticles, Wastewater, Kinetics

Citation: Sobhanardakani S, Zandipak R, Taghavi L. Synthesis of 2,4-dinitrophenylhydrazine loaded sodium dodecyl sulfate-coated magnetite nanoparticles for adsorption of Hg(II) ions from an aqueous solution. Environmental Health Engineering and Management Journal 2016; 3(4): 183–189. doi: 10.15171/EHEM.2016.18.

Article History:
Received: 23 June 2016
Accepted: 24 August 2016
ePublished: 15 September 2016

***Correspondence to:**
Soheil Sobhanardakani
Email: s_sobhan@iauh.ac.ir

Introduction

Recent industrial activity has increased the presence of hazardous heavy metals such as mercury (Hg) ions in wastewater (1). Hg (II) is hazardous to health and the environment and is extreme toxic, even at low levels. This element biomagnifies in the food chain and bioaccumulates in organisms (2). It exists in the environment in the form of inorganic mercury as metallic, mercurous (Hg_2^{2+}), mercuric (Hg^{2+}); and organic mercury containing methyl, ethyl and phenyl groups (3). The potential sources of Hg(II) ions in wastewater includes fungicides, the electronics industry, nonferrous metal smelting, metals used in manufacturing, paints, pigments and batteries (4).

Mercury can cause neurodegenerative diseases such as amyotrophic lateral sclerosis, Alzheimer disease and Parkinson disease. Elemental mercury and inorganic compounds damage the immune system and kidneys and methyl mercury can cause cardiovascular disease and nervous system disorders (5). The World Health Organization (WHO) sets the permissible limit of Hg(II) for drinking water at 0.001 mg L^{-1}.

Adsorption, coagulation-flocculation, ion-exchange, membrane filtration, chemical precipitation, flotation and electrochemical have all been employed for metal ion removal from aqueous solution; however, all these methods except adsorption are inefficient for the removal of some metal ions and incur high operational costs (6,7). Adsorption has been demonstrated to be the most efficient method for removal of heavy metal ions from

aqueous solutions (8,9).

Adsorbents such as chitosan, iron oxides, activated carbon and polymeric materials have been applied to remove heavy metal from wastewater; however, these adsorbents have shown low adsorption capacities or low rates of adsorption (10). Recently, magnetite nanoparticles (Fe_3O_4) have been tested as an efficient adsorbent. They offer a high surface area, magnetic response and the unique advantage of easy separation under external magnetic fields (11,12). To further facilitate the adsorption affinity, surface modification through physical coatings and covalent bonding has been explored to enable specific metal complexation (13).

The present work coated magnetite nanoparticles with sodium dodecyl sulfate (SDS), an anionic surfactant. Next, 2,4-dinitrophenylhydrazine (2,4-DNPH), an important reagent which can act as an electron pair donor to react with most hard and intermediate cations, was chemically immobilized on the surface of the SDS-coated magnetite nanoparticles and the product was used for adsorption of Hg(II) ions from an aqueous solution. The effects of pH, adsorbent dose and contact time on the adsorption efficiency were studied. The adsorption mechanisms are discussed in detail. The adsorption kinetic and isotherm were also investigated.

Methods

Apparatus and reagents

Hg(II) ion concentration was measured by cold vapor atomic absorption spectroscopy (CVAAS) using a direct mercury analyzer (DMA-80). Adjustments in pH were carried out using a pH meter (Metrohm; model 713; Switzerland). The adsorbent (DNPH@SDS@Fe_3O_4 nanoparticles) was characterized using scanning electron microscopy (SEM; Hitachi-S4160; Japan) and x-ray diffraction (XRD; Italstructure; ADP2000; Italy). Fourier transform infrared spectroscopy (FTIR) at 400 to 4000 cm^{-1} in KBr were recorded on a FTIR spectrometer (PerkinElmer; spectrum 100). The porosity and specific surface area were defined by N_2 adsorption–desorption porosimetry (77 K) using a porosimeter (MicrotacBEL; Japan).

All chemicals and reagents used in this work were of analytical grade and were purchased from Merck (Germany). Double-distilled water was used throughout the study. A stock solution of Hg(II) (1000 mg L^{-1}) was prepared by dissolving the appropriate amount of $Hg(NO_3)_2{\cdot}6H_2O$ in double-distilled water.

Synthesisof Fe_3O_4 nanoparticles

The magnetite nanoparticles were synthesized using the conventional co-precipitation method. Briefly, $FeCl_3.6H_2O$ (11.68 g) and $FeCl_2.4H_2O$ (4.30 g) were dissolved in 200 mL of double-distilled water under nitrogen gas in an ultrasonic bath at 85°C for a few minutes to produce smaller, more homogenous particles. Next, 20 mL of 30% NH_3 was added dropwise to the solution. The color of the suspension turned black immediately. The precipitated Fe_3O_4 nanoparticles were washed with ddH_2O and once with 0.02 mol L^{-1} NaCl and were separated using an external magnetic field (14).

Synthesis of magnetite modified with 2,4-DNHD sodium dodecyl sulfate

For this purpose, 2.0 g of magnetite nanoparticles were diffused in 50 mL of water and mixed with 100 mg of SDS. Next, 20 mL of a solution of 0.90 g 2,4-DNPH in concentrated hydrogen chloride + acetonitril was added. The suspension was stirred at 60°C for 3 hours and then the solvent was evaporated and the remaining produce was washed, air-dried, and stored in a closed bottle for subsequent use.

Point of zero charge of the DNPH@SDS@Fe_3O_4 nanoparticles (pH_{PZC})

The point of zero charge (PZC) is a characteristic of metal oxides (hydroxides) and is of fundamental importance to surface science. It relates to adsorption and describes the condition at which the electrical charge density on a surface is zero. The pH_{PZC} of the DNPH@SDS@Fe_3O_4 nanoparticles was determined in degassed 0.01 mol L^{-1} $NaNO_3$ solution at 20°C. Aliquots of 30 ml of 0.01 mol L^{-1} $NaNO_3$ were mixed with 30 mg of DNPH@SDS@Fe_3O_4 nanoparticles in several beakers. The pH of the solutions were adjusted to 2.0 to 9.0 using solutions of 0.01 mol L^{-1} of HNO_3 and/or NaOH as appropriate. The initial pH of the solutions were recorded and the beakers were covered with parafilm and shaken for 24 hours. The final pH values were recorded. The pH_{pzc} was recorded as the point at which $pH_{initial} = pH_{final}$.

Adsorption kinetics and equilibrium testing

Adsorption kinetics testing was carried out by adding 0.04 g of DNPH@SDS@Fe_3O_4 nanoparticles to three initial concentrations of Hg(II) (25, 50, 90 mg L^{-1}), which was then shaken at 150 rpm and 25°C. At specified time intervals, a strong permanent magnet used to separate the synthesized adsorbent. The concentration of the residual Hg(II) in the solution was measured by CVAAS using a DMA-80. The amount of metal adsorbed at each time interval per unit mass of the adsorbent q_t (mg g^{-1}) was calculated as:

$$q_t = \frac{(C_0 - C_t)V}{W} \quad (1)$$

where C_0 (mg L^{-1}) denotes the initial liquid-phase concentration of the metal, C_t (mg L^{-1}) denotes the concentration at time t, V (l) denotes the volume of the solution and W (g) denotes the mass of the adsorbent. Adsorption equilibrium testing was carried out by adding 0.04 g of DNPH@SDS@Fe_3O_4 nanoparticles to 15 ml of initial concentrations Hg(II) solution (25 to 420 mg L^{-1}). The samples were shaken for 24 hours to reach equilibrium, then the solution was analyzed for residual metal (Hg(II)) content using CVAAS on a DMA-80. The number of adspecies at equilibrium, q_e (mg g^{-1}), were

computed as:

$$q_e = \frac{(C_0 - C_e)V}{W} \quad (2)$$

where C_e (mg L^{-1}) denotes the metal concentration at equilibrium.

Results

Characterization of modified magnetite nanoparticles

In order to better understand the adsorption behavior of DNPH@SDS@Fe_3O_4 nanoparticles toward the metal ions, their structural properties were characterized. The XRD pattern of DNPH@SDS@Fe_3O_4 nanoparticles is shown in Figure 1. The SEM and SEM-EDX results of the Fe_3O_4 nanoparticlesare shown in Figure 2. Figure 3 shows the FTIR spectra of the DNPH@SDS@Fe_3O_4 nanoparticles.

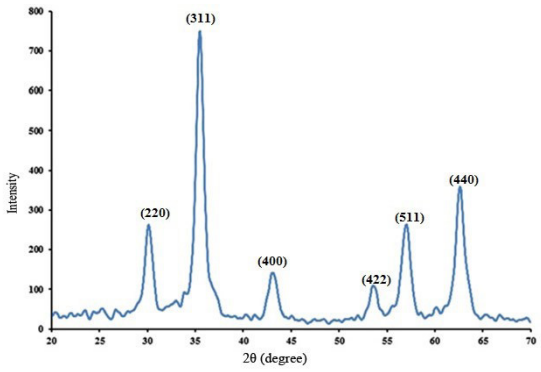

Figure 1. XRD patterns of Fe_3O_4 nanoparticles.

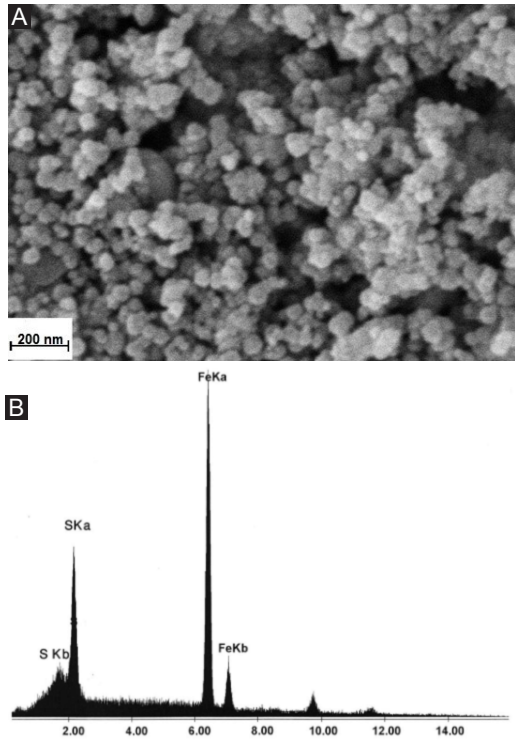

Figure 2. (A) SEM image of DNPH@SDS@Fe_3O_4 nanoparticles; (B) SEM-EDX spectrum of SDS@Fe_3O_4 nanoparticles.

Effect of solution pH

The PZC (pH_{pzc}) of the DNPH@SDS@Fe_3O_4 adsorbent was 5.0 (Figure 4A). The influence of pH on Hg(II) adsorption onto DNPH@SDS@Fe_3O_4 was studied at pH values ranging from 1.0 to 10 (Figure 4B). The maximum adsorption of Hg(II) onto DNPH@SDS@Fe_3O_4 occurred at about pH 7.0.

Effect of adsorbent dose

The relation between adsorbent dose and removal of Hg(II) ions by DNPH@SDS@Fe_3O_4 nanoparticles is shown in Figure 5. The percentage of Hg(II) removed increased as the dose of adsorbent increased from 0.01 to 0.04 g; thus, 0.04 g of adsorbent dose was selected as the optimum dose for the remaining experiments. Increasing the dose of

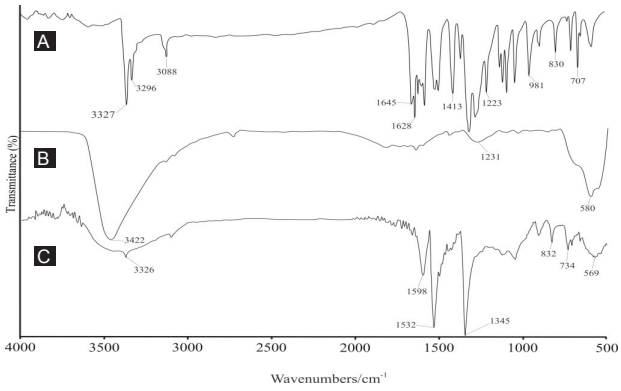

Figure 3. FTIR spectrum of: (A) 2,4-DNPH; (B) magnetite nanoparticles; (C)DNPH@SDS@Fe_3O_4nanoparticles

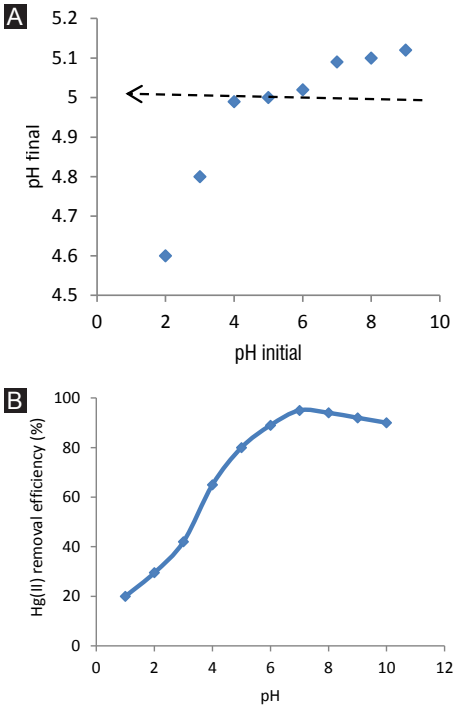

Figure 4. (A) PZC of DNPH@SDS@Fe_3O_4 nanoparticles; (B) effect of pH on the removal of Hg(II) ions (C_0= 25 mg l^{-1}, contact time = 45 min, dose of adsorbent = 0.04 g, temperature = 25°C).

adsorbent beyond this point did not appreciably increase Hg(II) adsorption.

Effect of shaking time and kinetics

The effect of contact time was determined at three concentrations of Hg(II) solution (5, 50 and 90 mg L^{-1}). The removal of Hg(II) from solution by DNPH@SDS@Fe_3O_4 as a function of contact time is shown in Figure 6. It is clear that the adsorption capacity of Hg(II) onto the DNPH@SDS@Fe_3O_4 nanoparticles increased as the contact time increased. Three kinetic models were tested to determine the adsorption kinetics of Hg(II) ions onto DNPH@SDS@Fe_3O_4 nanoparticles (Figure 7). The kinetic parameters are listed in Table 1.

Equilibrium

Freundlich and Langmuir equilibrium isotherms were used to determine the adsorption mechanism of DNPH@SDS@Fe_3O_4 for Hg(II) ions. The equilibrium isotherm for adsorption of Hg(II) ions onto the magnetite nanoparticles at pH 7.0 and 25°C is shown in Figure 8. The adsorption constants obtained from the isotherms are listed in Table 2.

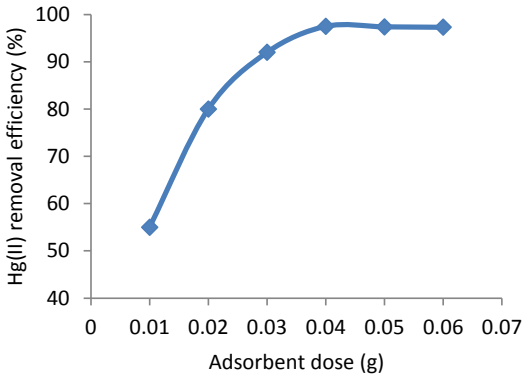

Figure 5. Effect of dose of DNPH@SDS@Fe_3O_4 nanoparticles on removal of Hg(II) ions (C_0= 25 mg l^{-1}, initial pH = 7.0, contact time = 45 min, temperature = 25°C).

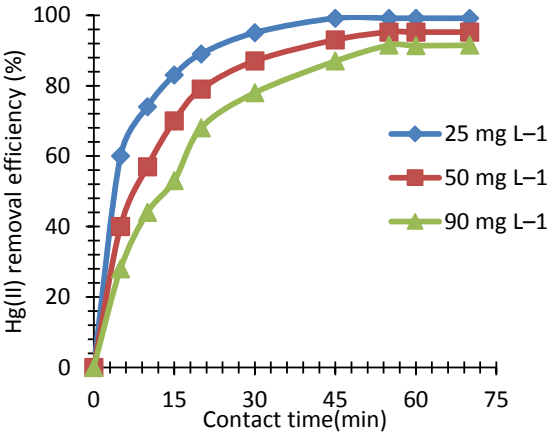

Figure 6. Effect of contact time on removal of Hg(II) ions (C_0= 25, 50 and 90 mg l^{-1}, initial pH = 7.0, dose of adsorbent = 0.04 g, temperature = 25°C).

Discussion

As shown in Figure 1, the XRD pattern of the magnetite is consistent with the six diffraction peaks at (220), (311), (400), (422), (511) and (440) recorded by the Joint Committee on Powder Diffraction Standards (JCPDS card, file No. 79-0418) indexed to the cubic spinel phase of Fe_3O_4. The XRD pattern confirms that the synthesized adsorbents are Fe_3O_4. The SEM image of the nanoparticles in Figure 2A shows an average diameter for DNPH@SDS@Fe_3O_4 nanoparticles of 20 to 35 nm with a spherical shape.

Typical SEM-EDX elemental analysis of SDS@Fe_3O_4 nanoparticles is shown in Figure 2B and shows the peak areas of Fe and S from which the atomic ratio of Fe/S was calculated to be 96.66/3.34 = 28.9. This represents the surface SDS coverage ratio of the adsorbent. An adjacent monolayer of the surface coating is the likely source of incompleteness of surface protonation and the existence of spatial resistance for the surface coating reaction.

The specific surface area was determined using the BET

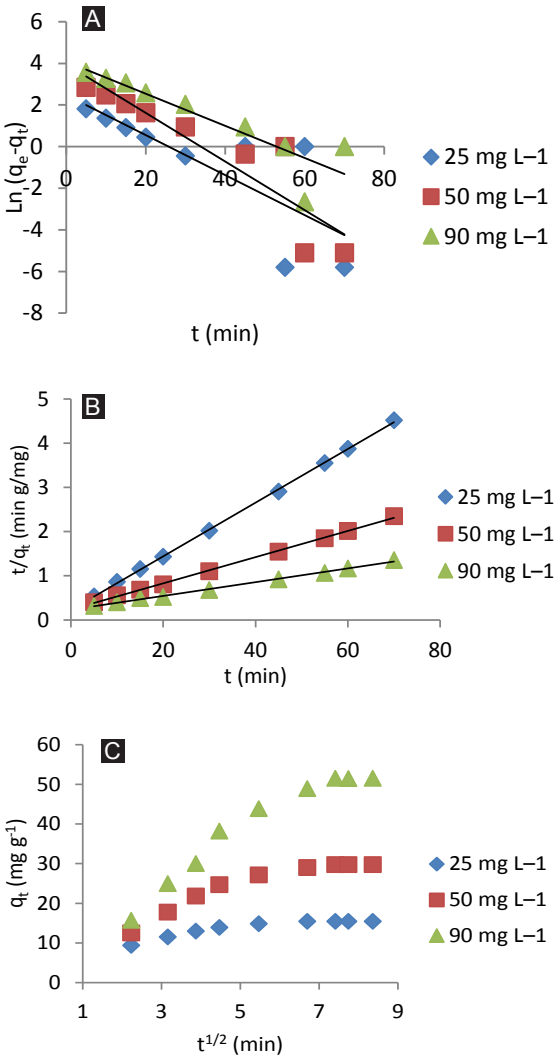

Figure 7. Adsorption of Hg(II) ions onto DNPH@SDS@Fe_3O_4 nanoparticles at 25°C: (A) pseudo-first-order kinetic; (B) pseudo-second-order kinetic; (C) intraparticle diffusion.

Table 1. Kinetic model parameters for adsorption of Hg(II) ions onto adsorbent at 25°C

C_0 (mg L^{-1})	q_e exp(mg g^{-1})	Pseudo-first-order			Pseudo-second-order			Intraparticle diffusion		
		q_{e1}(mg g^{-1})	k_1 (min^{-1})	R^2	q_{e2} (mg g^{-1})	k_2 (g mg^{-1} min^{-1})	R^2	K_{id} (mg g^{-1} $min^{-0.5}$)	A	R^2
25	15.69	11.88	0.096	0.618	16.47	0.016	0.999	0.909	8.851	0.836
50	30.28	52.24	0.116	0.830	33.78	0.003	0.998	2.652	10.14	0.877
90	60.22	59.38	0.077	0.808	64.10	0.001	0.998	5.855	7.433	0.932

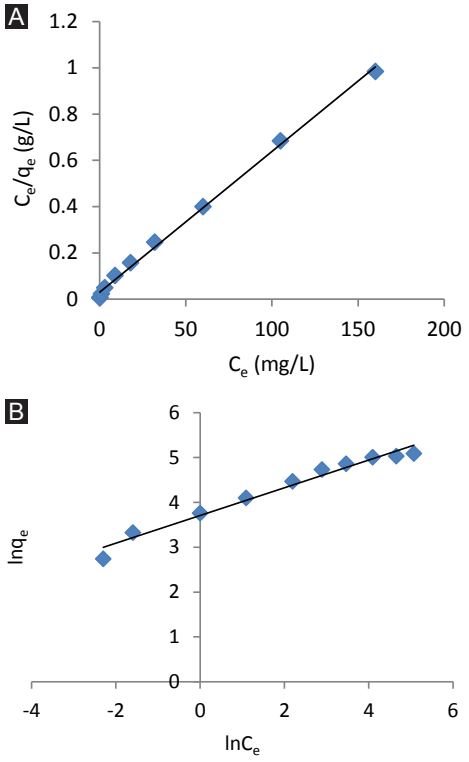

Figure 8. Equilibrium isotherms for adsorption of Hg(II) ions onto DNPH@SDS@Fe_3O_4 at 25°C: (A) Langmuir; (B) Freundlich.

Table 2. Isotherm parameters of adsorption of Hg(II) ions onto DNPH@SDS@Fe_3O_4 at 25°C

Langmuir			Freundlich		
b (L mg^{-1})	q_m (mg g^{-1})	R^2	K_f ($mg^{1-(1/n)}$ $l^{1/n}$ g^{-1})	n	R^2
0.206	164.0	0.996	40.77	3.237	0.972

equation applied to the adsorption data (15,16). The results showed that the average specific surface areas of the Fe_3O_4 and DNPH@SDS@Fe_3O_4 nanoparticles were 99.3 and 75.5 m^2 g^{-1}, respectively. It can be concluded from these values that this type adsorbent comprises nanoparticles with relatively large specific surface areas. The decrease in surface area of the adsorbent as compared to the magnetite nanoparticles may be the result of aggregation after modification with DNPH.

The FTIR spectra of the 2,4-DNPH, Fe_3O_4 nanoparticles and adsorbent are shown in Figures 3A, 3B and 3C, respectively. The Fe_3O_4 nanoparticles are evident from the occurrence of a strong absorption band in the FTIR spectrum which encompasses the characteristic wave number of 580 cm^{-1}. This pattern corresponds to Fe–Ovibrations in Fe_3O_4 (Figure 3B). After immobilization of 2,4-DNPH onto magnetite nanoparticles, a visible broadband of modified Fe_3O_4 nanoparticles appears in the 3200–3500 cm^{-1} region caused by stretching vibrations of N–H or OH groups with varying degrees of hydrogen bonding. The absorption spectrum shows absorption bands (cm^{-1}) at 1345, 1532 and 1598 that correspond to the bending vibrations of the N–H group (Figure 3C). Comparison of these characteristic spectral bands indicates that the surface-modified Fe_3O_4 nanoparticles contain the –NH–functional group.

Aqueous solution pH is an important controlling parameter in heavy metal adsorption. Figure 4B shows that an increase in pH from 2.0 to 7.0 increased adsorption of Hg(II) from 20% to 95%. The effect of solution pH could be explained by the ionization and surface charge of the adsorbate. The surface of the DNPH@SDS@Fe_3O_4 nanoparticles is covered with carboxyl, hydroxyl, and amino groups that vary in form at different pH values. At low pH (pH <pH_{pzc}), the groups on the surface are positively charged by protonation that causes electrostatic repulsion with the positively charged Hg(II) ions. As the pH increased (pH >pH_{pzc}), the number of negatively charged sites increased and the concentration of H_3O^+ decreased, weakening the competition between the positively charged H_3O^+ and mercury for the same functional groups, improving Hg(II) ion removal efficiency. Hg(II) speciation also favors adsorption at pH 7.0 due to the presence of Hg(II) species. Above pH 7.0, adsorption gradually decreased due to formation of $Hg(OH)_2$, which tends to precipitate at higher pH values. Similar behavior has been reported for Hg(II) adsorption on resin-loaded magnetic ß-cyclodextrin beads (3).

Figure 5 shows that an increase in adsorbent dose rapidly increased removal efficiency of Hg(II). Hg(II) adsorption increased from 55% at a dose of 0.01 g to 97.5% at a dose of 0.04 g of DNPH@SDS@Fe_3O_4 nanoparticles and did not further increase because the number of sites available for metal ion adsorption was limited. The increase in adsorption efficiency with an increase in adsorbent dose is likely the result of the increased number of binding sites available for the target pollutant (Hg(II)). It can be concluded that the optimum dose (0.04 g) of adsorbent provided sufficient adsorption sites for 97.5% adsorption efficiency under the experimental conditions. A value of 0.04 g of DNPH@SDS@Fe_3O_4 was thus selected as the optimum dose. These results are in agreement with the results of previous studies (17).

The adsorption of Hg(II) onto DNPH@SDS@Fe_3O_4 nanoparticles at different initial concentrations was

studied as a function of contact time to determine the adsorption equilibrium time. Initially, a large number of empty surface sites are available for adsorption that increase the rate of transfer and diffusion. After this stage, the appearance of strong repulsive forces and saturation of the pores and vacant surface sites with Hg(II) molecules on in solid and bulk phases decreases the migration and diffusion rates. Figure 6 shows that the contact time required for the Hg(II) solution at 25, 50 and 90 mg L^{-1} to reach equilibrium was 45, 55 and 55 minutes, respectively. The removal rate significantly decreased with an increase in initial Hg(II) concentrations from 25 to 90 mg L^{-1}.

To evaluate the kinetics of adsorption, the experimental results were compared with those predicted by the pseudo-first-order, pseudo-second-order and the intraparticle diffusion models. The pseudo-first-order model was described by Lagergren (18) as:

$$\ln(q_e - q_t) = \ln(q_e) - \frac{k_1 t}{2303} \quad (3)$$

where: q_e (mg g^{-1}) and q_t (mg g^{-1}) denote the adsorption capacity at equilibrium and at time t (min), respectively and k_1 (min^{-1}) denotes the rate constant of the pseudo-first-order kinetic model. The linear form of the pseudo-second-order kinetic model can be expressed as (18):

$$\frac{t}{q_t} = \frac{1}{k_2 q_e^2} + \frac{t}{q_e} \quad (4)$$

where: q_t (mg g^{-1}) denotes the adsorption uptake at time t (min) and k_2 (g $mg^{-1}min^{-1}$) denotes the rate constant of the pseudo-second order kinetic model.

The intraparticle diffusion model proposed by Weber and Morris was used to identify the mechanism involved in adsorption as (19):

$$q_t = k_{id} t^{0.5} + A \quad (5)$$

where K_{id} (mg $g^{-1}min^{-0.5}$) denotes the intraparticle diffusion rate constant and A (mg g^{-1}) is a constant denoting the thickness of the boundary layer.

The kinetic constants and correlation coefficient (R^2) of Hg(II) adsorption onto DNPH@SDS@Fe_3O_4 are presented in Table 1. As shown, R^2 indicates a better fit for the pseudo-second-order model to the experimental data than the other models (Figure 7). The low k_2 values (0.016, 0.003 and 0.001 g mg^{-1} min^{-1}) indicate that the rate of Hg(II) adsorption is rapid. Moreover, the q_e values for the pseudo-second-order model were similar to those for the experimental q_e (Table 1). It is reasonable to conclude that the rate limiting step during adsorption is chemisorption involving valence forces through the sharing or exchange of electrons between the metal ions and the adsorbent.

Figure 7C indicates that the data points are related in three stages. First, the adsorption rate is high, which can be imputed to external surface adsorption during which the Hg(II) diffuses through the solution to the external surface of the adsorbent or the boundary layer diffusion of the solute molecules. In the second stage, adsorption slows during the intraparticle diffusion as the rate-controlling step. The third stage is the final equilibrium phase during which intraparticle diffusion slows and levels off either because the remaining metal content is extremely low in solution or maximum adsorption has been attained.

Adsorption isotherm models explain the relationship between adsorbents and adsorbates (Hg(II)) at equilibrium. The adsorption isotherms of Hg(II) onto the DNPH@SDS@Fe_3O_4 nanoparticles were tested at a pH of 7.0 at different initial Hg(II) concentrations (25 to 420 mg L^{-1}). The Langmuir (20) and Freundlich (21) equations are shown in Eqs. (6) and (7), respectively:

$$\frac{C_e}{q_e} = \frac{C_e}{q_m} + \frac{1}{q_m b_1} \quad (6)$$

$$\ln q_e = \frac{1}{n} \ln C_e + \ln k_f \quad (7)$$

where c_e (mg L^{-1}) denotes the equilibrium concentration of adsorbate ions in solution, q_e (mg g^{-1}) denotes the equilibrium adsorption capacity of the adsorbent, q_m (mg g^{-1}) denotes the maximum adsorption capacity of adsorbent for monolayer coverage, b (L mg^{-1}) is a constant related to adsorption free energy, K_f ($mg^{1-(1/n)}$ $L^{1/n}$ g^{-1}) is a constant related to adsorption capacity, and n is an empirical parameter related to adsorption.

The results indicate that the linear correlation coefficient for the Langmuir model (R^2= 0.996) was higher than the Freundlich model (R^2= 0.972), but the Langmuir model fitted the adsorption information better than the Freundlich model. It confirms that the adsorption occurs in a monolayer and that the adsorption of each molecule has equal activation energy. It is clear that adsorption occurs on a homogeneous surface. The maximum adsorption capacity using the Langmuir model was 164.0 mg g^{-1} at 25°C.

Hg(II) adsorption capacity was compared with the results of other adsorbents from previous studies. The adsorption capacities of thiol-modified Fe_3O_4@SiO_2 was 148.8 (22), resin-loaded magnetic ß-cyclodextrin beads was 88.4 (3), grapheme oxide was 80.7 (5) and chitosan was 52.6 (23); however, a higher adsorption capacity and better removal efficiency were recorded for the DNPH@SDS@Fe_3O_4 nanoparticles prepared in this work.

Conclusion

DNPH@SDS@Fe_3O_4 nanoparticles were synthesized and used for adsorption of Hg(II) ions from aqueous solutions. The BET surface area of the adsorbent was 75.5 m^2 g^{-1}, which can facilitate diffusion and adsorption of Hg(II) onto the adsorbent. An acceptable adsorption efficiency for Hg(II) was observed as the initial pH of the solution varied from 1.0 to 7.0. The mechanism for Hg(II) adsorption can be explained by the electrostatic interaction of the negatively charged surfaces of DNPH@SDS@Fe_3O_4 nanoparticles and Hg(II) species. Hg(II) adsorption followed pseudo-second-order kinetics. Equilibrium data were well-described by the Langmuir isotherm, suggesting that adsorption occurred mainly in

a monolayer. The results show that DNPH@SDS@Fe_3O_4 nanoparticles are an economic adsorbent for removal of Hg(II) ions from aqueous solution.

Acknowledgments

The authors are grateful to the Hamedan Branch, Islamic Azad University for providing the facilities to conduct and complete this study.

Ethical issues

The authors certify that all data collected during the study is presented in this manuscript and no data from the study has been or will be published separately.

Competing interests

The authors declare that they have no competing interests.

Author contributions

All authors participated in the study design, literature search, writing of the manuscript, and data acquisition, analysis, and interpretation. All authors critically reviewed, refined, and approved the manuscript.

References

1. Cegłowski M, Schroeder G. Preparation of porous resin with Schiff base chelating groups for removal of heavy metal ions from aqueous solutions. Chem Eng J 2015; 263: 402-11. doi: 10.1016/j.cej.2014.11.047.
2. Cui L, Wang Y, Gao L, Hu L, Yan L, Wei Q, et al. EDTA functionalized magnetic graphene oxide for removal of Pb (II), Hg (II) and Cu (II) in water treatment: adsorption mechanism and separation property. Chem Eng J 2015; 281: 1-10. doi: 10.1016/j.cej.2015.06.043.
3. Cui L, Wang Y, Gao L, Hu L, Wei Q, Du B. Removal of Hg(II) from aqueous solution by resin loaded magnetic β-cyclodextrin bead and graphene oxide sheet: synthesis, adsorption mechanism and separation properties. J Colloid Interface Sci 2015; 456: 42-9. doi: 10.1016/j.jcis.2015.06.007.
4. Wang Z, Xu J, Hu Y, Zhao H, Zhou J, Liu Y, et al. Functional nanomaterials: Study on aqueous Hg(II) adsorption by magnetic Fe_3O_4@SiO_2-SH nanoparticles. Journal of the Taiwan Institute of Chemical Engineers 2016; 60: 394-402. doi: 10.1016/j.jtice.2015.10.041.
5. Fan Q, Yang Y, Hao Y, Zhao X, Feng Y. Preparation of three-dimensional PANI/GO for the separation of Hg(II) from aqueous solution. J Mol Liq 2015; 212: 557-62. doi: 10.1016/j.molliq.2015.10.008.
6. Al-Zoubi H, Ibrahim KA, Abu-Sbeih KA. Removal of heavy metals from wastewater by economical polymeric collectors using dissolved air flotation process. J Water Process Eng 2015; 8: 19-27. doi: 10.1016/j.jwpe.2015.08.002.
7. Zhang Z, Zhang H, Zhu L, Zhang Q, Zhu W. Hierarchical porous Ca $(BO_2)_2$ microspheres: hydrothermal–thermal conversion synthesis and their applications in heavy metal ions adsorption and solvent-free oxidation of benzyl alcohol. Chem Eng J 2016; 283: 1273-84. doi: 10.1016/j.cej.2015.08.073.
8. Sobhanardakani S, Parvizimosaed H, Olyaie E. Heavy metals removal from wastewaters using organic solid waste—rice husk. Environ Sci Pollut Res Int 2013; 20(8): 5265-71. doi: 10.1007/s11356-013-1516-1.
9. Zandipak R, Sobhanardakani S. Synthesis of $NiFe_2O_4$ nanoparticles for removal of anionic dyes from aqueous solution. Desalin Water Treat 2015; 57(24): 11348–60. doi: 10.1080/19443994.2015.1050701.
10. Sun Y, Yue Q, Gao B, Gao Y, Xu X, Li Q, et al. Adsorption and cosorption of ciprofloxacin and Ni(II) on activated carbon-mechanism study. J Taiwan Inst Chem Eng 2014; 45(2): 681-8. doi: 10.1016/j.jtice.2013.05.013.
11. Afkhami A, Moosavi R. Adsorptive removal of Congo red, a carcinogenic textile dye, from aqueous solutions by maghemite nanoparticles. J Hazard Mater 2010; 174(1-3): 398-403. doi: 10.1016/j.jhazmat.2009.09.066.
12. Lai L, Xie Q, Chi L, Gu W, Wu D. Adsorption of phosphate from water by easily separable Fe_3O_4@SiO_2 core/shell magnetic nanoparticles functionalized with hydrous lanthanum oxide. J Colloid Interface Sci 2016; 465: 76-82. doi: 10.1016/j.jcis.2015.11.043.
13. Wang J, Zheng S, Shao Y, Liu J, Xu Z, Zhu D. Amino-functionalized Fe_3O_4@ SiO_2 core–shell magnetic nanomaterial as a novel adsorbent for aqueous heavy metals removal. J Colloid Interface Sci 2010; 349(1): 293-9. doi: 10.1016/j.jcis.2010.05.010.
14. Sobhanardakani S, Zandipak R. 2, 4-Dinitrophenylhydrazine functionalized sodium dodecyl sulfate-coated magnetite nanoparticles for effective removal of Cd (II) and Ni (II) ions from water samples. Environ Monit Assess 2015; 187(7): 412. doi: 10.1007/s10661-015-4635-y.
15. Brunauer S, Emmett PH, Teller E. Adsorption of gases in multimolecular layers. J Am Chem Soc 1938; 60(2): 309-19. doi: 10.1021/ja01269a023.
16. Venkatesha T, Viswanatha R, Nayaka YA, Chethana B. Kinetics and thermodynamics of reactive and vat dyes adsorption on MgO nanoparticles. Chem Eng J 2012; 198-199: 1-10. doi: 10.1016/j.cej.2012.05.071.
17. Shan C, Ma Z, Tong M, Ni J. Removal of Hg(II) by poly (1-vinylimidazole)-grafted Fe_3O_4@SiO_2 magnetic nanoparticles. Water Res 2015; 69: 252-60. doi: 10.1016/j.watres.2014.11.030.
18. Azizian S. Kinetic models of sorption: a theoretical analysis. J Colloid Interface Sci 2004; 276(1): 47-52. doi: 10.1016/j.jcis.2004.03.048.
19. Ghaedi M, Biyareh MN, Kokhdan SN, Shamsaldini S, Sahraei R, Daneshfar A, et al. Comparison of the efficiency of palladium and silver nanoparticles loaded on activated carbon and zinc oxide nanorods loaded on activated carbon as new adsorbents for removal of Congo red from aqueous solution: Kinetic and isotherm study. Mater Sci Eng C 2012; 32(4): 725-34. doi: 10.1016/j.msec.2012.01.015.
20. Langmuir I. The adsorption of gases on plane surfaces of glass, mica and platinum. J Am Chem Soc 1918; 40(9): 1361-403. doi: 10.1021/ja02242a004.
21. Freundlich H, Heller W. The adsorption of cis-and trans-azobenzene. J Am Chem Soc 1939; 61(8): 2228-30. doi: 10.1021/ja01877a071.
22. Zhang S, Zhang Y, Liu J, Xu Q, Xiao H, Wang X, et al. Thiol modified Fe_3O_4@ SiO_2 as a robust, high effective, and recycling magnetic sorbent for mercury removal. Chem Eng J 2013; 226: 30-8. doi: 10.1016/j.cej.2013.04.060.
23. Sobhanardakani S, Zandipak R, Javanshir-Khoei A, Hosseini SM, Moslemi M, Delfieh P. Removal of Hg (II) and Cd (II) Ions from aqueous solution using chitosan: kinetics and equilibrium studies. Iran J Health Sci 2015; 3(2): 21-30. doi: 10.7508/ijhs.2015.02.004.